

Original Research Article

Calculated Torque Control of a Planar Parallel Robot 2-RR

Eugenio Yime Rodríguez^{1*}, Javier Roldán Mckinley¹, José Villa Ramírez²

¹ Universidad del Atlántico, Grupo DIMER, Barranquilla, Colombia

² Universidad Tecnológica de Bolívar, Grupo GAICO, Cartagena de Indias, Colombia

ABSTRACT

This paper introduces the design, structure and control method of a five-bar planar mechanism with five revolute joints and two degrees of freedom. The control is realized by calculating the torque in the joint space to obtain the required trajectory. The direct and inverse kinematics of position and velocity are proposed, and the inverse kinematics of acceleration is taken as the parameter required by the control law. The method selected for this parallel robot is advantageous because it allows to obtain the dynamic equations similar to the traditional series robot modeling, which is helpful to the realization of nonlinear control technology. The effectiveness of the method and the functionality of the controller are verified by experiments, and a circular trajectory is generated by the actuator. Although the simulation results are consistent with the experimental results, it is suggested that the future work is to change the control strategy to compensate for the influence of the unmodeled system.

Keywords: CTC; Parallel Dynamics; Robot Control; 5-Bar Mechanism; Planar Robot 2-RR

ARTICLE INFO

Received: Mar 11, 2022

Accepted: Apr 21, 2022

Available online: May 3, 2022

*CORRESPONDING AUTHOR

Eugenio Yime Rodríguez
eugenioyime@mail.uniatlantico.edu.co;

CITATION

Yime Rodríguez E, Roldán Mckinley J, Villa Ramírez J. Calculated torque control of a planar parallel robot 2-RR. Journal of Autonomous Intelligence 2021; 5(1): 72-84. doi: 10.32629/jai.v5i1.508

COPYRIGHT

Copyright © 2022 by author(s) and Frontier Scientific Publishing. This work is licensed under the Creative Commons Attribution-NonCommercial 4.0 International License (CC BY-NC 4.0).
<https://creativecommons.org/licenses/by-nc/4.0/>

1. Introduction

The five-bar mechanism is one widely studied in mechanism and machinery literature^[1-4], partly because of its simple structure and easy manufacture. It is widely used in the research of kinematics and dynamics of planar mechanism. Some studies using this mechanism include using it as a function generator^[5], trajectory generator^[6], motion design of task related links^[7], and various robot applications^[8-10]. A particularly interesting application of robotics in this mechanism is its use for the rehabilitation of patients with upper limb disabilities^[11].

From the perspective of kinematics, the topological structure of the five-bar mechanism is characterized by two kinematic chains composed of rotating joints, the first of which is the driven joint, so it is named 2-RR^[12,13]. The five bar mechanism is an ideal mechanical system to study the basic theoretical concepts of parallel robot dynamics, dynamics and control. An example of this is Quanser's distributed teaching platform, which is named "2-DOF Robot"^[14]. However, despite the problem of commercialization, it is still necessary to build a system in line with the needs of the times to study this problem. In this regard, research shows DEXTAR's development in the laboratories of the École de Technologie Supérieure (ÉTS), Canada^[15,16]; it is used for sports school alignment^[13], and then for minimum time trajectory control^[17].

With regard to system control, a control method for hybrid performance is described^[8], that is, a DC motor with speed control on one joint and a servo motor with position control on another degree of freedom of the system. Research shows various nonlinear control

techniques applied to five bar mechanisms^[18-20]. See literature^[21,22] for other examples of hybrid performance control. The control progress of five-bar planar mechanism also enables it to be used in teleoperation applications of parallel robots, such as the PAROLA laboratory^[23], which has a five-bar manipulator, Delta robot and 3-RRR robot. Other challenges in controlling the mechanism are proposed in the case of flexible link actuator positioning, which is realized through the research on QFT control and model-based vibration suppression control^[24,25].

This paper introduces the first part of the ongoing research on the five-bar mechanism at the Universidad Tecnológica de Bolívar, Cartagena, Colombia. This report includes design, construction, modeling and control. The first section describes the implementation of the design and the construction of the prototype. Then, the kinematics and dynamics models are introduced. The latter is realized by the method used by Stewart Gough space robot in space mission, but this paper is developed in joint space. It is consistent with the simulation of calculated torque control and the experiment of calculated torque dynamic control.

2. Methodology

2.1 Description of the prototype

The mechanism was manufactured at the Universidad Tecnológica de Bolívar using CNC milling machines, ordinary lathes and drill bits. The system uses two 60 W Maxon Motor RE30 actuators with 66:1 reduction, and 500 pulses per revolution encoder. The connecting rod is made of aluminum, processed on a HAAS TM-1P milling machine, and made of 2-inch wide and 1/2-inch thick pressing plates. **Figure 1** shows the CAD model of the assembly developed in SolidEdge, while **Figure 2** shows the prototype of the final assembly. **Table 1** summarizes the dimensions of the mechanism links.

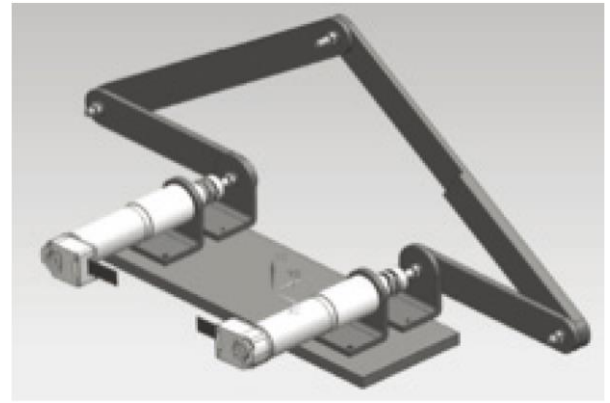


Figure 1. Mechanical CAD model.



Figure 2. Built prototype.

Table 1. Link lengths

Link	1	2	3	4	5
Length (mm)	200	150	300	300	150
Width (mm)	-	30	30	30	30
Thickness (mm)	-	6	10	10	6

2.2 Position kinematics

Figure 3 shows the terminology used in the kinematic analysis of the five-bar mechanism. The inertial reference frame is located at point A, and points B, C, D and P are used to define the position of the swivel. Point P further defines the desired position of the mechanism, that is, the position of the end effector. The vectors, where i is from 1 to 5, are used to determine the position and direction of each link. The angle θ_i defines the rotation of the connecting rod relative to the x-axis. The position of the center of gravity of each link is given by the vector, and the rotation angle of the vector relative to each vector is expressed by β_i . Position analysis includes inverse kinematics, which is usually used for end effector motion planning, and direct kinematics, which is used to close the end effector position control loop. The naming of the

definition allows the vector equation of the loop to be established in equation (1), as shown in **Figure 3**.

$$r_1 + r_2 + r_3 = r_5 + r_4 \quad (1)$$

2.2.1 Inverse position kinematics

The five-bar mechanism has two degrees of freedom, so it is necessary to control two actuators to define the position of the actuator. Inverse kinematics is responsible for calculating the value of the driven joints, θ_2 and θ_5 , as a function of the desired position of point P and the other parameters of the mechanism. The left side of the loop in equation (1) can be written in its components to generate the scalar equation given in equations (2) and (3), knowing that the components of point P are P_x and P_y .

$$P_x = L_1 + L_2 c_2 + L_3 c_3 \quad (2)$$

$$P_y = L_2 s_2 + L_3 s_3 \quad (3)$$

where $c_i = \cos\theta_i$ and $s_i = \sin\theta_i$. By abstracting for θ_2 from equations (2) and (3) after canceling the terms of the angle θ_3 by squaring both sides of equations (2) and (3), finding the sum term to term, and substituting it into the identity of the mean angular tangent to obtain the equation (4),

$$\theta_2 = 2 \tan^{-1} \left(\frac{B_2^2 + C_2^2 - A_2^2}{2(A_2 + C_2)} \right) \quad (4)$$

where $A_2 = 2(L_1 - P_x)L_2$, $B_2 = -2P_yL_2$, $C_2 = L_3^2 - L_1^2 - L_2^2 - P_x^2 - P_y^2 + 2L_1P_x$.

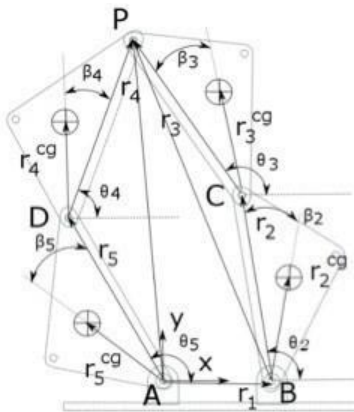


Figure 3. Labeling for kinematic analysis.

Similarly, in order to obtain the expression of θ_5 , the initial equations (4) and (5) are obtained through elements 4 and 5 from the origin of the inertial frame to the actuator point P.

$$P_x = L_5 c_5 + L_4 c_4 \quad (5)$$

$$P_y = L_5 s_5 + L_4 s_4 \quad (6)$$

By abstracting θ_5 from equations (5) and (6), equation (7) can be obtained.

$$\theta_5 = 2 \tan^{-1} \left(\frac{B_5 + \sqrt{B_5^2 + C_5^2 - A_5^2}}{2(A_5 + C_5)} \right) \quad (7)$$

where $A_5 = 2L_5P_x$, $B_5 = 2L_5P_y$, $C_5 = L_5^2 - L_4^2 + P_x^2 + P_y^2$.

By resolving the vector equation (1), the remaining position angle is obtained, and by repeating the trigonometric method, the position angle is obtained,

$$\theta_3 = 2 \tan^{-1} \left(\frac{B_3 + \sqrt{B_3^2 + C_3^2 - A_3^2}}{2(A_3 + C_3)} \right) \quad (8)$$

where $A_3 = 2L_3r_x$, $B_3 = 2L_3r_y$, $C_3 = L_4^2 - L_3^2 - r_x^2 - r_y^2$, and

$$\theta_4 = 2 \tan^{-1} \left(\frac{B_4 + \sqrt{B_4^2 + C_4^2 - A_4^2}}{2(A_4 + C_4)} \right) \quad (9)$$

where $A_4 = 2L_4r_x$, $B_4 = 2L_4r_y$, $C_4 = L_4^2 - L_3^2 + r_x^2 + r_y^2$.

2.2.2 Direct position kinematics

For the direct kinematics of position, the coordinates of point P are calculated through the information provided by the encoders located in the actuators, angles θ_2 and θ_5 , and the fulfillment of equations (2) and (5) for P_x , and equations (3) and (6) for P_y is verified.

2.3 Velocity kinematics

Velocity analysis is used to link the speed of actuators 2 and 5 with the velocity of the end effector V_p . As in

position analysis, there are direct kinematics analysis and inverse kinematics analysis.

2.3.1 Inverse velocity kinematics

When exporting equations (2) and (3), equations (10) and (11) can be obtained, which relate the velocity of the end effector to the angular velocities of links 2 and 3, respectively.

$$V_{p,x} = -L_2\omega_2s_2 - L_3\omega_3s_3 \quad (10)$$

$$V_{p,y} = L_2\omega_2c_2 + L_3\omega_3c_3 \quad (11)$$

Deleting ω_3 from the system of equations (10) and (11) yields the velocity ratio between the end effector and the actuated link 2, as shown in equation (12), with $s_{i-j} = \sin(\theta_i - \theta_j)$.

$$\omega_2 = -V_{p,x} \frac{c_3}{L_2s_{2-3}} - V_{p,y} \frac{s_3}{L_2s_{2-3}} \quad (12)$$

Similarly, θ_2 is removed from equations (10) and (11) to relate the angular velocity of link 3 to the velocity of the end effector, given in equation (13).

$$\omega_3 = V_{p,x} \frac{c_2}{L_3s_{2-3}} + V_{p,y} \frac{s_2}{L_2s_{2-3}} \quad (13)$$

In order to relate angular velocities ω_4 and ω_5 to the end-effector velocity V_p , equations (5) and (6) are derived to generate equations (14) and (15).

$$V_{p,x} = -L_4\omega_4s_4 - L_5\omega_5s_5 \quad (14)$$

$$V_{p,y} = L_4\omega_4c_4 + L_5\omega_5c_5 \quad (15)$$

The angular velocities ω_5 and ω_4 from the system of equations (14) and (15) as a function of the effector velocity to obtain equations (16) and (17), respectively.

$$\omega_5 = -V_{p,x} \frac{c_4}{L_5s_{5-4}} - V_{p,y} \frac{s_4}{L_5s_{5-4}} \quad (16)$$

$$\omega_4 = V_{p,x} \frac{c_5}{L_4s_{5-4}} + V_{p,y} \frac{s_5}{L_5s_{5-4}} \quad (17)$$

2.3.2 Inverse Jacobian

Equations (12) and (16) containing the ratios of change of the actuated links 2 and 5, respectively, are grouped to find inverse Jacobian of velocities, J^{-1} , by equation (18), where the velocity of point P V_p is expressed in the equation (19). The velocity vector of the actuated joints is ω given in the equation (20). The inverse Jacobian connects the angular velocity of the actuator with the velocity of the end actuator and is derived from the equation (18) and clearly presented in equation (21).

$$\omega = J^{-1}V_p \quad (18)$$

$$V_p = [V_{p,x}^T V_{p,y}^T]^T \quad (19)$$

$$\omega = [\omega_2 \omega_5]^T \quad (20)$$

$$J^{-1} = \begin{bmatrix} \frac{c_3}{L_2s_{3-2}} & \frac{s_3}{L_2s_{3-2}} \\ \frac{c_4}{L_5s_{4-5}} & \frac{s_4}{L_5s_{4-5}} \end{bmatrix} \quad (21)$$

2.3.3 Direct movement velocity

Now we have an expression that relate the angular velocities ω_3 and ω_4 to the end-effector velocity V_p , as a function of the known angular velocities of the actuators ω_2 and ω_5 . Starting with the derivative of equations (2), (3), (5) and (6) with respect to time, they are equalized by components to obtain equations (22) and (23).

$$-L_2\omega_2s_2 - L_3\omega_3s_3 = -L_5\omega_5s_5 - L_4\omega_4s_4 \quad (22)$$

$$L_2\omega_2c_2 + L_3\omega_3c_3 = L_4\omega_4c_4 + L_5\omega_5c_5 \quad (23)$$

The known velocities are ω_2 and ω_5 , so the angular velocity ω_4 can be eliminated from the system of

equations (22) and (23) to obtain the expression for ω_3 given in equation (24).

$$\omega_3 = \left(\omega_5 \frac{L_5}{L_3} - \omega_2 \frac{L_2}{L_3} \right) \frac{s_{4-2}}{s_{4-3}} \quad (24)$$

Similarly, ω_2 is deleted from equations (22) and (23) to find the expression for ω_4 in the equation (25).

$$\omega_4 = \left(\omega_2 \frac{L_2}{L_3} - \omega_5 \frac{L_5}{L_4} \right) \frac{s_{3-2}}{s_{3-4}} \quad (25)$$

By replacing equations (24) and (25) in equations of (10) and (11), and (14) and (15), the relationship between the end-effector velocities and the input angular velocities are obtained. By rearranging the items and considering that the results must be the same, because it is the same output variable with the same input variable, the expression of the end-effector velocities in the coordinates x and y can be obtained, presented in equations (26) and (27), respectively.

$$V_{p,x} = \omega_2 \frac{L_2 s_4 s_{2-3}}{s_{3-4}} + \omega_5 \frac{L_5 s_3 s_{4-5}}{s_{3-4}} \quad (26)$$

$$V_{p,y} = \omega_2 \frac{L_2 s_4 s_{2-3}}{s_{3-4}} - \omega_5 \frac{L_5 s_3 s_{4-3}}{s_{3-4}} \quad (27)$$

2.3.4 Jacobian

Equation (18) can be rewritten as shown in equation (28), and the Jacobian expression of the system J shown in the equation (29) can be determined, that is, a matrix that links the tool speed to the speed of the actuated joints. Equation (29) is consistent with the inverse solution of the equation (21) as expected.

$$V_p = J\omega \quad (28)$$

$$J = \begin{bmatrix} \frac{L_2 s_4 s_{2-3}}{s_{3-4}} & \frac{L_5 s_3 s_{4-5}}{s_{3-4}} \\ \frac{L_2 c_4 s_{2-3}}{s_{4-3}} & \frac{L_5 c_3 s_{4-5}}{s_{4-3}} \end{bmatrix}$$

$$(29)$$

2.3.5 Jacobian links

The Jacobian of the connecting rod $J_{\theta,i}$ represented by is used in the dynamic model to connect the center of gravity velocity of each connecting $V_{cg,i}$ rod with the angular velocity of the actuator, which is expressed as the velocity vector of ω the joint shown in the equation (20). The general expression for link i is shown in the equation (30).

$$V_{cg,i} = J_{\theta,i}\omega \quad (30)$$

For link 2, the center of gravity speed is determined by

$$V_{cg,2} = \begin{bmatrix} V_{cg,2x} \\ V_{cg,2y} \end{bmatrix} \quad (31)$$

With a given velocity component

$$V_{cg,2x} = -\omega_2 r_2^{cg} s_{2+\beta_2} \quad (32)$$

$$V_{cg,2y} = \omega_2 r_2^{cg} s_{2+\beta_2} \quad (33)$$

where $s_{i+\beta_i} = \sin(\theta_i + \beta_i)$ and $c_{i+\beta_i} = \cos(\theta_i + \beta_i)$.

From equations (32) and (33), the Jacobian of the second link can be derived in the equation (34).

$$J_{\theta,2} = \begin{bmatrix} -r_2^{cg} s_{2+\beta_2} & 0 \\ r_2^{cg} c_{2+\beta_2} & 0 \\ 1 & 0 \end{bmatrix} \quad (34)$$

Similarly, for the centroid velocity of the fifth connecting rod, equations in (35) and (36) are established, from which the Jacobian of the fifth link, presented in equation (37) can be deduced.

$$V_{cg,5x} = -\omega_5 r_5^{cg} s_{5+\beta_5} \quad (35)$$

$$V_{cg,5y} = \omega_5 r_5^{cg} c_{5+\beta_5}$$

(36)

$$J_{\theta,5} = \begin{bmatrix} 0 & -r_5^{cg} s_{5+\beta 5} \\ 0 & r_5^{cg} c_{5+\beta 5} \\ 0 & 1 \end{bmatrix}$$

(37)

For the third link, the center of gravity velocity is calculated by equations (38) and (39).

$$V_{cg,3x} = -\omega_2 L_2 s_2 - \omega_3 r_3^{cg} s_{3+\beta 3}$$

(38)

$$V_{cg,3y} = \omega_2 L_2 c_2 + \omega_3 r_3^{cg} c_{3+\beta 3}$$

(39)

When replacing equation (24) in equations (38) and (39), the velocity components of the center of mass of the third link are expressed in terms of the actuated joints to obtain the third Jacobian, given by,

$$J_{\theta,3} = \begin{bmatrix} \frac{L_2 r_3^{cg} s_{243}}{L_3 s_{3-4}} - L_2 s_2 & \frac{L_5 r_3^{cg} s_{453}}{L_3 s_{3-4}} \\ L_2 c_2 - \frac{L_2 r_3^{cg} s_{243}}{L_3 s_{3-4}} & -\frac{L_5 r_3^{cg} s_{453}}{L_3 s_{3-4}} \\ \frac{L_2 s_{4-2}}{L_3 s_{3-4}} & \frac{L_2 s_{4-2}}{L_3 s_{3-4}} \end{bmatrix}$$

(40)

where $ss_{243} = s_{2-4}s_{3+\beta 3}$, $ss_{453} = s_{4-5}s_{3+\beta 3}$, $sc_{243} = s_{2-4}c_{3+\beta 3}$, $sc_{453} = s_{4-5}c_{3+\beta 3}$.

Finally, for connecting rod 4, the expression of center of gravity velocity is expressed in equations (41) and (42).

$$V_{cg,4x} = -\omega_5 L_5 s_5 - \omega_4 r_4^{cg} s_{4+\beta 4}$$

(41)

$$V_{cg,4y} = \omega_5 L_5 c_5 + \omega_4 r_4^{cg} c_{4+\beta 4}$$

(42)

By replacing the equations (25) in equations (41) and (42) after rearranging the items, we get

$$J_{\theta,4} = \begin{bmatrix} \frac{L_2 r_4^{cg} s_{244}}{L_4 s_{3-4}} & \frac{L_5 r_4^{cg} s_{354}}{L_4 s_{3-4}} \\ -\frac{L_2 r_4^{cg} s_{244}}{L_4 s_{3-4}} & L_5 c_5 - \frac{L_5 r_4^{cg} s_{344}}{L_4 s_{3-4}} \\ \frac{L_2 s_{3-2}}{L_4 s_{3-4}} & -\frac{L_5 s_{3-5}}{L_4 s_{3-4}} \end{bmatrix}$$

(43)

where $ss_{244} = s_{2-4}s_{4+\beta 4}$, $ss_{354} = s_{3-5}s_{4+\beta 4}$, $sc_{244} = s_{2-4}c_{4+\beta 4}$, $sc_{354} = s_{3-5}c_{4+\beta 4}$.

2.4 Inverse kinematics acceleration

Since the dynamic formula will be based on the principle of virtual work, the dynamic analysis is transformed into the derivation of the Jacobian derivative of the connecting rod. However, for the calculated torque control, it is necessary to know the expected acceleration of the driven joint, which is one of the disadvantages of this control strategy. Then, it is necessary to carry out reverse acceleration analysis to determine the expected acceleration of the joint from the expected acceleration of the end effector. By deriving equation (18), the expression of the acceleration of the acting joint and the acceleration of the end effector given in (44) is obtained.

$$\alpha = J^{-1}A_p + J^{-1}V_p$$

(44)

This term can be obtained either by explicitly deriving the inverse Jacobian expression of equation (21) and multiplying the result by the end-effector velocity; or by clearing the corresponding item from the derivative of equations (10) and (11); and (14) and (15), in which case the expression given in the equations (45) is obtained.

$$J^{-1}V_p = \begin{bmatrix} \frac{L_2 \omega_2^2 c_{3-2} + L_3 \omega_3^2}{L_2 s_{3-2}} \\ \frac{L_5 \omega_5^2 c_{4-5} + L_4 \omega_4^2}{L_5 s_{4-5}} \end{bmatrix}$$

(45)

2.5 Dynamic analysis

Using the same method as that used by Stewart Gough space parallel robot in space task^[26,27], the dy-

dynamic analysis of planar five-bar parallel robot is carried out; the dynamic model in this paper is calculated in the joint space. The dynamic equation is represented by the model:

$$\tau_\theta = M_\theta(\theta)\ddot{\theta} + C_\theta(\theta, \dot{\theta})\dot{\theta} + g_\theta(\theta) \quad (46)$$

where M , C and g are generalized mass matrix, Coriolis matrix and gravitational vector in joint space respectively, and are generalized or external force (and/or moment) vectors. In calculating these terms, the contribution of each link should be taken into account, as follows:

$$M_\theta = \sum J_{\theta,i}^T M_i J_{\theta,i} \quad (47)$$

$$C_\theta = \sum J_{\theta,i}^T C_i J_{\theta,i} + \sum J_{\theta,i}^T M_i \dot{J}_{\theta,i} \quad (48)$$

$$g_\theta = \sum J_{\theta,i}^T g_i \quad (49)$$

Among them, M_i , C_i and g_i represent the mass matrix, Coriolis and gravity vector matrices, of each link expressed in the reference frame of its center of gravity. For the five-bar mechanism, the Coriolis matrix represented by the center of gravity is null, $C_i = [0]$, because it is a planar mechanism, but the mass matrix and gravity vector do exist. The format of the quality matrix for each link is:

$$M_i = \begin{bmatrix} m_i & 0 & 0 \\ 0 & m_i & 0 \\ 0 & 0 & I_{zz} \end{bmatrix} \quad (50)$$

where, m_i is the mass of the link and I_{zz} is the moment of inertia of the link around the axis perpendicular to the two-dimensional plane of the robot. The gravity vector of each link, g_i , shall be determined by the gravity vector expression in the mechanism reference system, as shown in **Figure 3**. It defines the gravitational $g = [g_x; g_y; 0]^T$ vector and helps to define the gravitational

vector of each link given in equation (51).

$$g_i = m_i g \quad (51)$$

Finally, the matrix $J_{\theta,j}$ represents the Jacobian of the links previously proposed in equations (34), (37), (40) and (43), matrices represent their derivatives. In dynamic modeling, obtaining these items may be the most cumbersome, especially for matrices linking 3 and 4. However, if symbolic processing software such as Mathematica or maple is used to generate the expressions of mass matrix, Coriolis and gravity vector, the dynamic algorithm is relatively easy to program. The results can be output to Matlab for simulation of control algorithm, and can also be directly output to C language for programming of embedded control system.

2.6 Calculated torque control

Computational torque control is an ideal nonlinear control method for robot control based on dynamic model. The method is summarized in the literature^[28, 29]. Starting from the dynamic model equation (52), a way is sought to eliminate the nonlinear term of Coriolis and gravity, and establish a control law, namely equation (53), where is the expected acceleration vector on the connecting rod and u is the acceleration error variable defined by the equation (54), then expressed explicitly by equation (55) according to the error vector e , its change rate and positive definite matrix K_p and K_v , thus simplifying the expression to equation (56).

$$\tau = M\dot{q} + C\dot{q} + g \quad (50)$$

$$\tau = M(\ddot{q}_d + u) + C\dot{q} + g \quad (51)$$

$$u = \ddot{q} - \ddot{q}_d \quad (52)$$

$$u = K_p e + k_v \dot{e} \quad (53)$$

$$\ddot{e} + K_p e + k_v \dot{e} = 0 \quad (54)$$

Substitution equation (55) in the equation (53) allows to express the control law:

$$\tau = M(\ddot{q}_d + K_p e + K_v \dot{e}) + C\dot{q} + g \quad (57)$$

However, this paper adopts the following format:

$$\tau = M_\theta(\alpha_d + K_p(\tilde{\theta}) + K_v(\tilde{\omega})) + C_\theta\omega + g_\theta \quad (58)$$

where, α_d is the required joint acceleration vector, and defined the joint angular velocity error vectors, expressed respectively by equations (59) and (60).

$$\tilde{\theta} = \theta_d - \theta \quad (57)$$

$$\tilde{\omega} = \omega_d - \omega$$

2.7 Calculation and simulation

The simulation is carried out in Simulink to verify the established dynamic model and the control law to be realized. **Figure 4** shows the control architecture used. The task to be performed is the circular motion of the robot end effector. The trajectory scheduler outputs the required point, linear velocity and acceleration according to the simulation time. These data are transferred to inverse kinematics, which calculates the position θ_i , velocity ω_i and angular acceleration α_i of each connecting rod and transmits the results to the controller. The block calculates a position error $\theta_d - \theta$ and velocity error matrix that $\omega_d - \omega$ converts the mass of M_θ , the Coriolis matrix C_θ , and the gravity vector g_θ for subsequent evaluation of the control law in equation (58).

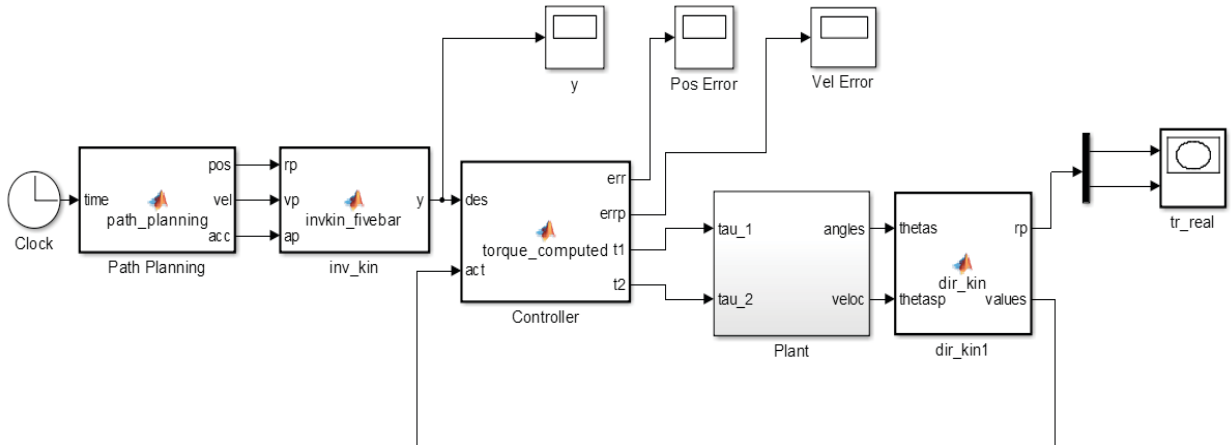


Figure 4. Blocks for Simulink simulation.

The controller calculates the torque of each motor and transmits the results to a module in Simmechanics, which performs the direct dynamic simulation of the system by returning the joint position of the input link. Finally, the motion block performs direct motion according to the information provided by the actuator to evaluate the position and speed of the current system. To facilitate viewing the task, use the model in **Figure 6**. The CAD model of the mechanism is established by using Siemens NX10, and the mass, inertia and center of gravity position of each connecting rod in Simmechanics are

obtained. The dimensions of the link are shown in **Table 1**, while the dynamic characteristics used in the simulation are shown in **Table 2**. As shown in the CAD system design **Figure 3**, the angle β_i used to locate the center of gravity of each connecting rod must be zero. The simulation was performed for gain values set at $K_p = 20I_{2 \times 2}$ and $K_v = 10I_{2 \times 2}$. Gravity is on the y -axis and has a value of -9.8 m/s^2 . Since the friction at the joint is not simulated, a constant K_v is required in the simulation. The results are shown in **Figures 7, 8, 9** and **10**.

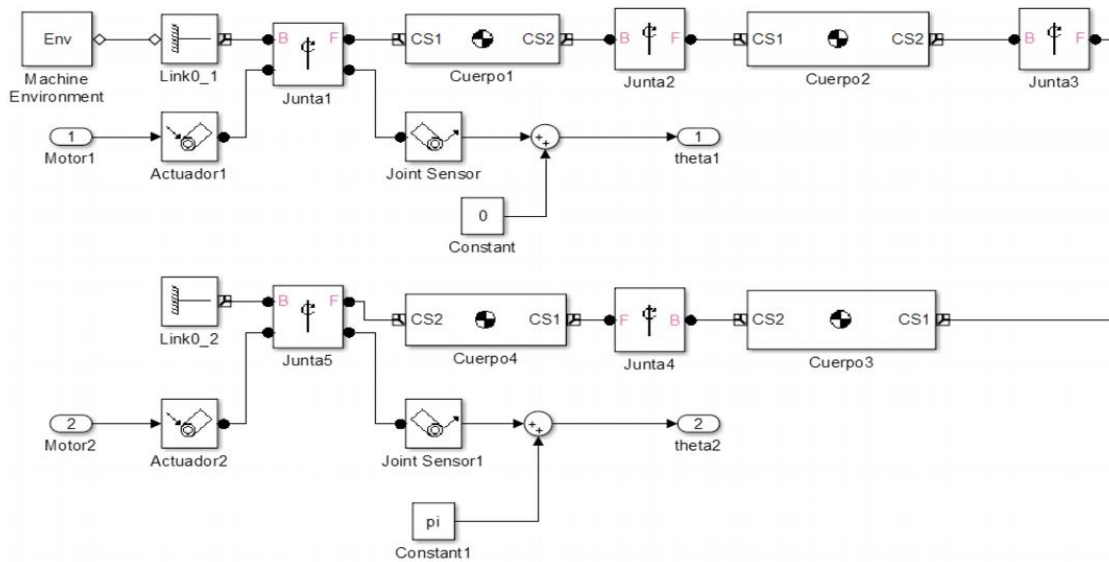


Figure 5. SimMechanics robot model.

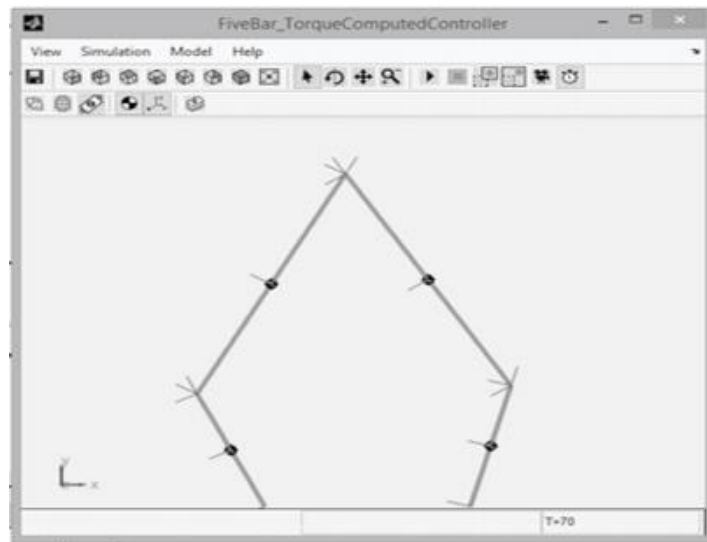


Figure 6. Simmechanics view.

Table 2. Link properties.

Link	Mass [kg]	Inertia [kg-mm ²]	r_i^{cg} [mm]
2	0.079	186.95	80.43
3	0.196	1589.29	124.92
4	0.194	1517.91	122.84
5	0.079	186.95	80.43

As can be seen from **Figure 7**, the required trajectory is a circle with a diameter of 100 mm, and the center is [77.5; 350; 0] mm, which is slightly different from the trajectory generated by the robot in the simulation. **Figure 8** illustrates the positioning error of the actuator. The maximum tracking error is 0.014 rad. **Figure 9** shows the

angular velocity error of the actuator, and the maximum velocity tracking error is 0.008 rad/s. The torque required for the engine to operate is shown in **Figure 10**. The maximum torque required is 0.4 N-m for engine 1 acting on gasket 2 and -0.4 N-m for engine 2 acting on gasket 5.

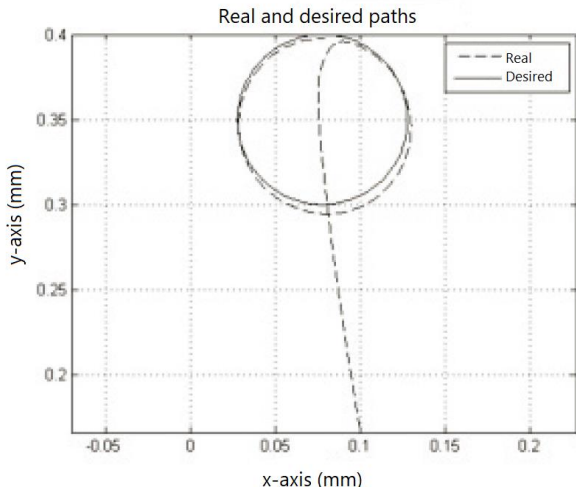


Figure 7. Real and simulated paths.

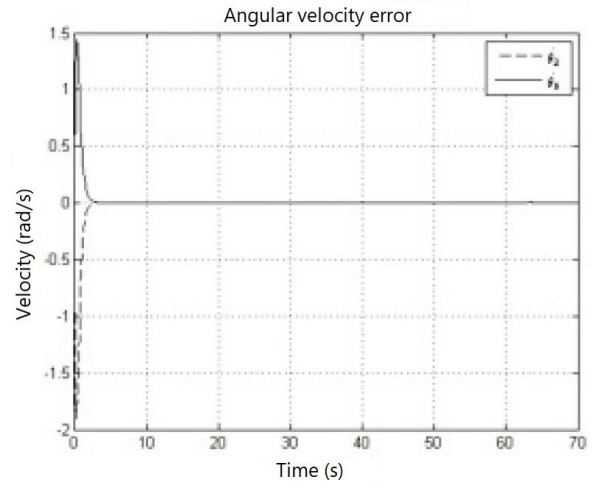


Figure 9. Joint velocity errors.

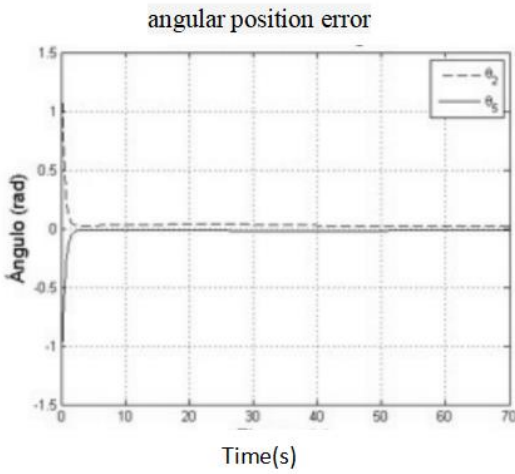


Figure 8. Activation joint errors.

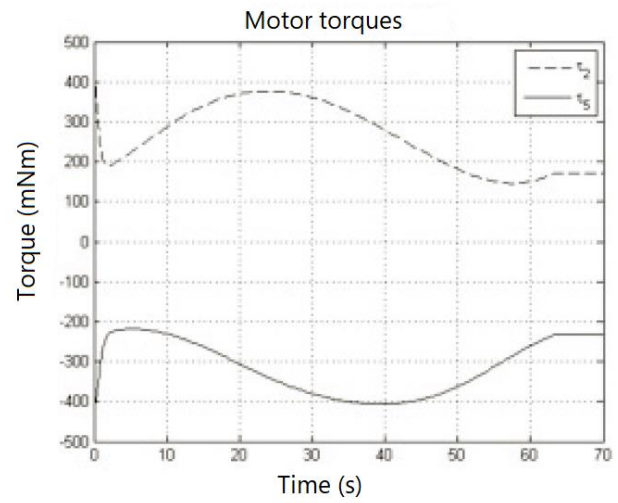


Figure 10. Motors torques.

3. Results and discussion

The control system is installed on the PC-104 embedded card, Advantech reference PCM-3362N-S6A1E. The card is connected to the PC-104 bus through a sensor card 526 with four analog outputs and four encoder inputs. The operating system is Linux, 64 bit Debian Jessie, and Pengutronix distributed real-time kernel is added^[30]. The control system is connected to the Maxon EPOS 2 24/2 amplifier. The torque constant K_t of Maxon Motors is 25.9 mN-m/A, which means that using reducer GP-32, the deceleration rate is 66:1, and the average efficiency is 50%. The motor reducer assembly can provide a maximum continuous torque of 1.7 N-m.

The control algorithm is designed in Matlab and

output to C language with codegen tool of Matlab. The main program on Linux is based on the real-time application example, which is located on the RT PREEMPT patch page^[31]. The control is performed at a priority of 49 and a frequency of 1000 Hz.

Because the friction of the system and the mechanical deviation from the theoretical model are small, it is necessary to add an integral part to the calculated torque controller. The final values of the constants used are $K_p = 100I_{2 \times 2}$, $K_v = 500I_{2 \times 2}$ and $K_i = 10I_{2 \times 2}$. From the theoretical simulation, it can be seen that the friction between joints plays an important role in the test part, which explains the constant K_p and K_v .

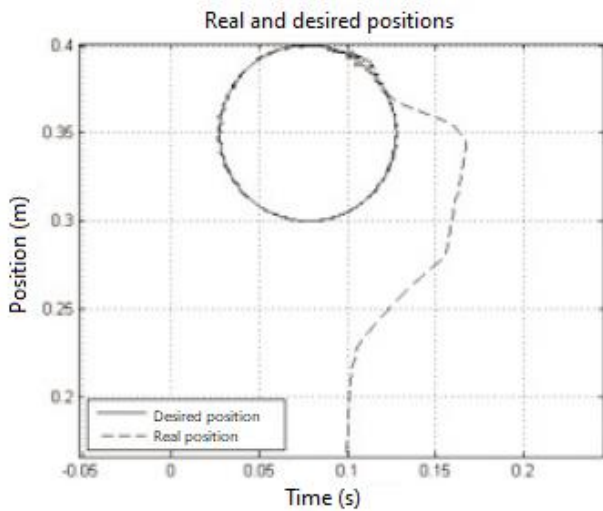


Figure 11. Real robot trajectories.

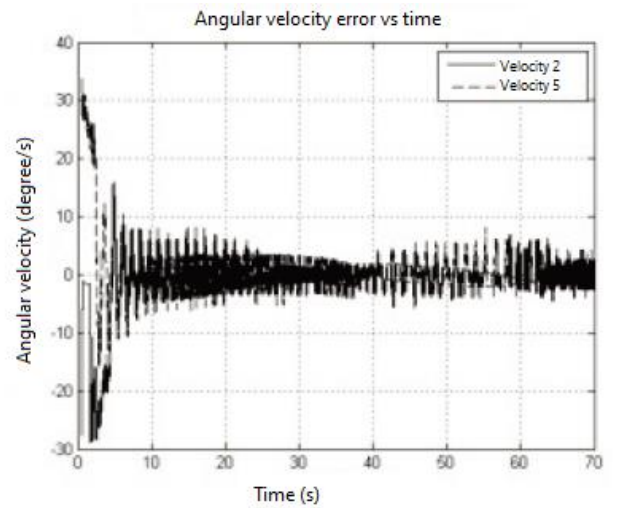


Figure 13. Joint velocity errors.

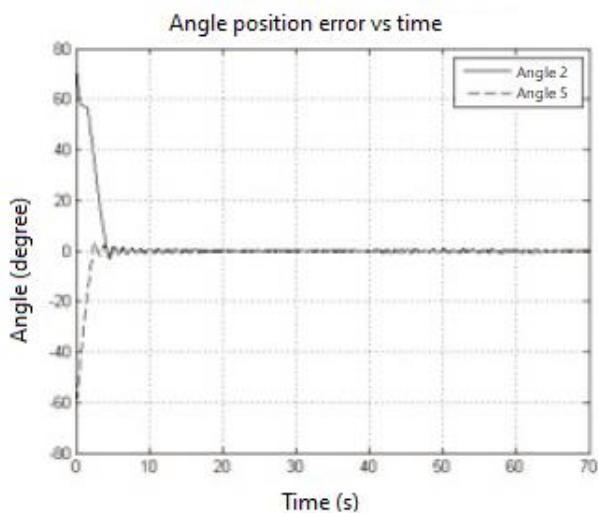


Figure 12. Joint position errors.

Figure 11 shows the actual trajectory executed by the robot end effector. It points out that there is an obvious tracking error initially, which decreases after 3 seconds (within [5,8] s), which can be better seen in Figure 12. This figure illustrates the actual angular position error of the robot. Starting from the initial position of 0° of joint 2 and 180° of joint 5, it can be seen that the maximum position error during circular trajectory tracking is 5° .

Figure 13 shows the angular velocity error of joints 2 and 5 during the experiment. The form of angular velocity error simulation is similar, as shown in Figure 9. The maximum error recorded in the tracking phase is $5\%/s$. Finally, Figure 14 shows the torque on joints 2 and 5, and the noise caused by friction can be seen.

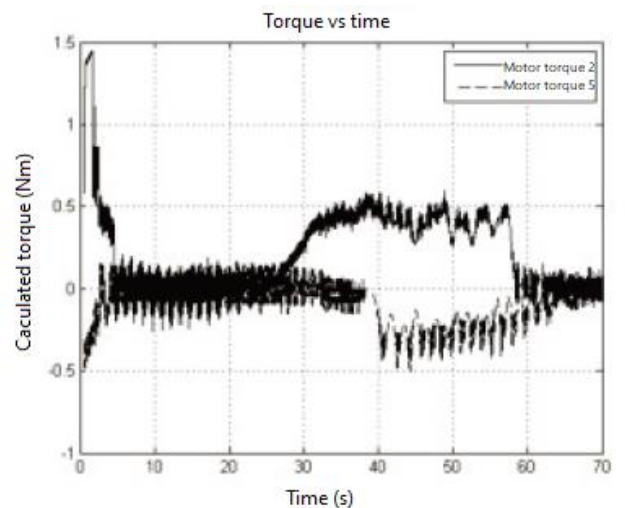


Figure 14. Real joint torques.

4. Conclusion

The application of computational torque control technology in planar 2-DOF parallel robot is introduced. Computational torque control is suitable for nonlinear systems and requires an explicit dynamic model of the robot. The calculation model is an ideal calculation model for torque control, because it is a complete model, including the dynamic contribution of each link in the kinematic chain. Through simulation calculation, the effectiveness of the proposed control algorithm is verified, and a small tracking error is given. Experiments confirm that the tracking error needs to increase the proportion and velocity constant used in the simulation, because the controller does not consider the unmodeled terms of the dynamic equation, such as friction.

From the consistency between the experimental results and the experimental results, the scheme is satisfactory, but in the future work, it is proposed to apply other nonlinear

control strategies to the same trajectory, and its performance is compared.

References

1. Vinogradov O. Fundamentals of kinematics and dynamics of machines and mechanisms. U.S.A: CRC Press; 2000.
2. Uicker J, Pennock G, Shigley J. Theory of machines and mechanisms. U.S.A: Oxford University Press; 2010.
3. Norton R. Design of machinery: An introduction to the synthesis and analysis of mechanisms and machines. New York: McGraw-Hill; 2011.
4. Stanisic M. Mechanisms and machines: Kinematics, dynamics and synthesis. U.S.A: Cengage Learning; 2014.
5. Seth B, Vaddi S. Programmable function generator—I: Base five-bar mechanism. *Mechanism and Machine Theory* 2003; 38(4): 321–330. doi: 10.1016/S0094-114X(02)00121-0.
6. Zhou H, Ting KL. Path generation with singularity avoidance for five-bar slider-crank parallel manipulators. *Mechanism and Machine Theory* 2005; 40(3): 371–384. doi: 10.1016/j.mechmachtheory.2004.07.007.
7. Kim JY. Task based kinematic design of a two DOF manipulator with a parallelogram five-bar link mechanism. *Mechatronics* 2006; 16(6): 323–329. doi: 10.1016/j.mechatronics.2006.01.004.
8. Ouyang PR, Li Q, Zhang WJ, *et al.* Design, modeling and control of a hybrid machine system. *Mechatronics* 2004; 14(10): 1197–1217. doi: 10.1016/j.mechatronics.2004.06.004.
9. Nahavandi S, Uddin MJ, Saadat M, *et al.* Heavy tools manipulation by low powered direct-drive five-bar parallel robot. *Mechanism and Machine Theory* 2008; 43(11): 1450–1461. doi: 10.1016/j.mechmachtheory.2007.11.004.
10. Giberti H, Cinkemani S, Ambrosetti S. 5R 2-DOF parallel kinematic manipulator: A multidisciplinary test case in mechatronics. *Mechatronics* 2013; 23(8): 949–959. doi: 10.1016/j.mechatronics.2012.09.006.
11. Krebs H, Ferraro M, Buerger S, *et al.* Rehabilitation robotics: Pilot trial of a spatial extension for MIT-Manus. *Journal of NeuroEngineering and Rehabilitation* 2004; 1(5): 1–15. doi: 10.1186/1743-0003-1-5.
12. Villarreal-Cervantes M, Cruz-Villar C, Alvarez-Gallegos J, *et al.* Differential evolution techniques for the structure-control design of a five-bar parallel robot. *Engineering Optimization* 2010; 42(6): 535–565. doi: 10.1080/03052150903325557.
13. Joubair A, Slamani M, Bonev I. Kinematic calibration of a five-bar planar parallel robot using all working modes. *Robotics and Computer-Integrated Manufacturing* 2013; 29(4): 15–25. doi: 10.1016/j.rcim.2012.10.002.
14. Qunser. Two DOF robot [Online]. 2014 [Cited 2015 July 7]. Available from: http://www.quanser.com/Products/2dof_robot.
15. Figielski A, Bonev I, Bigras P. Towards development of a 2-DOF planar parallel robot with optimal workspace use. 2007 IEEE International Conference on Systems, Man and Cybernetics; 2007 Oct 7–10; Montreal. 2008. p. 1562–1566.
16. Campos L, Bourbonnais L, Bonev I, *et al.* Development of five-bar parallel robot with large workspace. ASME International Design Engineering Technology Conference; 2010 Aug 15–18; Montreal. 2010.
17. Bourbonnais F, Bigras P, Bonev I. Minimum time trajectory planning and control of a pick-and-place five-bar parallel robot. *IEEE/ASME Transactions on Mechatronics* 2015; 20(2): 740–749. doi: 10.1109/TMECH.2014.2318999.
18. Wu FX, Zhang WJ, Li Q, *et al.* Control of hybrid machines with 2-DOF for trajectory tracking problems. *IEEE Transactions on Control Systems Technology* 2005; 13(2): 338–342. doi: 10.1109/TCST.2004.839580.
19. Cheng L, Lin Y, Hou ZG, *et al.* Adaptive tracking control of hybrid machines: A closed-chain five-bar mechanism case. *IEEE/ASME Transactions on Mechatronics* 2011; 16(6): 1155–1163. doi: 10.1109/TMECH.2010.2083680.
20. Cheng L, Hou ZG, Tan M, *et al.* Tracking control of a closed-chain five-bar robot with two DOF by integration of an approximation-based approach and mechanical design. *IEEE Transactions on Systems, Man, and Cybernetics* 2012; 42(5): 1470–1479. doi: 10.1109/TSMCB.2012.2192270.
21. Zi B, Cao J, Zhu Z. Dynamic simulation of hybrid-driven planar five-bar parallel mechanism based on SimMechanics and tracking control. *International Journal of Advanced Robotic Systems* 2011; 8(4): 28–33. doi: 10.5772/45683.
22. Yu H. Modeling and control of hybrid machine systems—A five-bar mechanism case. *International Journal of Automation and Computing* 2006; 3(3): 235–243.
23. Peidro A, Gil A, Marín JM, *et al.* A web-based tool to analyze the kinematics and singularities of parallel robots. *Journal of Intelligent & Robotic Systems* 2015; 81(1): 145–163.
24. Karande S, Paluri N, Gandhi P, *et al.* Control of parallel flexible five-bar manipulator using QFT. *IEEE International Conference on Industrial Technology*; 2009 Feb;

- Gippsland. IEEE International; 2009.
25. Stacella K, Schreiber F, Schumacher W. Modeling, control, and evaluation of an experimental adaptronic five-bar robot. In: Schutz D, Wahl F (editors). Robotic systems for handling and assembly. Berlin: Springer Tracts in Advanced Robotics; 2001. p.125–142.
 26. Yime E, Saltaren R, Diaz J. (June 2010). Robust adaptive control of the Stewart-Gough robot in the task space. Proceedings of the 2010 American Control Conference; 2010 Jun; Baltimore. 2010. p. 5248–5253.
 27. Yime E, Saltaren R, García C, *et al.* Robot based on task-space dynamical model. IET Control Theory and Applications 2011; 5(18): 2111–2119. doi: 10.1049/iet-cta.2010.0622.
 28. Slotine JJE, Li WP. Applied nonlinear control. U.S.A: Prentice Hall; 1991.
 29. Siciliano B, Khatib O (editors). Springer handbook of Robotics. U.S.A: Springer International Press; 2008.
 30. Pengutronix. Real time kernel: Linux community distribution [Online]. 2016. [Cited 2016 Jun 28]. Available from: <http://debian.pengutronix.de/>.
 31. Fu L, Schwebel R. RT-preempt patch [Online] 2014. [Cited 2016 Jun 28]. Available from: [https://rt.wiki.kernel.org/index.php/RT PREEMPT HOWTO](https://rt.wiki.kernel.org/index.php/RT_PREEMPT_HOWTO).